© APR 2026 | IRE Journals | Volume 9 Issue 10 | ISSN: 2456-8880
DOI: https://doi.org/10.64388/IREV9I10-1716426

Solar PV Based Electric Vehicle Charging Station Using MATLAB/Simulink

DR. D. SRILATHA[1], PERAM VISHNUVARDHAN REDDY[2], PERAVALI SANDEEP[3], SHAIK SAMEER JAN[4], SHAIK ABDUL REHAMAN[5], SHAIK THOUFIQ HUSSAIN[6]
[1]*Professor, Department of EEE &Vasireddy Venkatadri Institute of Technology, India*
[2, 3, 4, 5, 6]*UG Students, Department of EEE &Vasireddy Venkatadri Institute of Technology, India*

Abstract- ***Electric vehicle charging stations built on solar PV face two problems that rarely get addressed together. The first is MPPT quality: fixed-step algorithms like Perturb and Observe cannot stop oscillating at steady state, so they waste a small but consistent fraction of available energy indefinitely. The second appears when a Thermoelectric Generator is added for waste heat recovery — connecting TEG output to the same battery as the PV charging path generates transient current spikes that destabilize charging. This paper takes both problems on in a single MATLAB/Simulink simulation. A 25-rule Mamdani Fuzzy Logic MPPT controller replaces the conventional fixed-step algorithm; it adjusts the Boost Converter duty cycle based on the power-voltage slope and its rate of change, and the result is a single startup transient followed by zero steady-state ripple. The Boost Converter output settles to roughly 715 V under nominal irradiance and dips briefly to around 695 V when an irradiance step hits at t = 1.0 s, recovering within a fraction of a second. The TEG feeds a dedicated auxiliary battery through a blocking diode rather than sharing the main battery terminal, which removes the cross-source interference entirely. Five simulation outputs — PV power, converter voltage, main battery SOC, auxiliary battery SOC, and combined battery current — all confirm stable and clean operation across the full two-second test window including the disturbance.***

Keywords: Solar PV; Electric Vehicle Charging; Fuzzy Logic MPPT; Thermoelectric Generator; Dual Battery; Boost Converter; MATLAB/Simulink; Waste Heat Recovery

I. INTRODUCTION

Charging an electric vehicle from a coal-heavy grid reduces tailpipe emissions but does not solve the carbon problem — it moves it upstream. Solar panels at or near the charging station avoid this by generating electricity from sunlight directly, and at current module prices the economics work for both grid-tied and off-grid configurations. The engineering is not trivial, but it is tractable, and the two problems this paper addresses are good examples of the kind of detail that matters in practice.

The first is maximum power point tracking. Solar panel output shifts continuously with irradiance and temperature, and the power-voltage curve has a single maximum that moves with those shifts. Tracking it requires an algorithm that can follow the MPP as it moves. The two algorithms most commonly deployed — Perturb and Observe and Incremental Conductance — apply a fixed perturbation step to the duty cycle and observe the resulting power change. The step size is the problem. A large step tracks fast but never stops oscillating around the MPP; a small step reduces the oscillation but slows convergence and costs energy during transients [1], [2]. There is no fixed step size that solves both. Fuzzy Logic MPPT escapes this trade-off by computing a correction that is large when the operating point is far from the MPP and shrinks toward zero as the MPP is approached — which is exactly the behavior a variable-step algorithm needs [4].

The second problem is what happens when a Thermoelectric Generator is added. Solar panels convert roughly 15 to 20 percent of incident irradiance into electricity; the rest becomes heat that actually reduces conversion efficiency by raising cell temperature. A TEG mounted on the panel rear surface can recover some of that heat through the Seebeck effect and deliver supplementary electrical energy. The trouble is that connecting TEG output to the same battery as the PV charging path puts two independent sources on a shared terminal. When their relative power levels shift — during startup, during irradiance changes, or just from normal TEG voltage variation — the battery sees current spikes that disrupt charging and complicate battery management system logic. A

separate auxiliary battery for the TEG output, isolated by a blocking diode, removes the shared terminal entirely.

This paper builds and simulates the full system in MATLAB/Simulink: Fuzzy Logic MPPT, DC-DC Boost Converter, Thermoelectric Generator, blocking diode, and a dual battery arrangement with one battery per source. Five output waveforms are analyzed — PV output power, Boost Converter output voltage, main battery SOC, auxiliary battery SOC, and combined battery current — and the results are compared against what a conventional fixed-step system would produce.

II. LITERATURE SURVEY

A. MPPT Algorithms

Esram and Chapman [1] compared more than nineteen MPPT techniques and found that Incremental Conductance outperforms Perturb and Observe on steady-state accuracy, though both share the fixed-step limitation. Femia et al. [2] showed that making the step size variable based on the power-voltage slope substantially improves performance and set the theoretical groundwork for intelligent MPPT methods. Subudhi and Pradhan [3] confirmed across a systematic comparison that soft-computing controllers consistently deliver better tracking efficiency and lower steady-state error than fixed-step alternatives. Rezk and Eltamaly [4] implemented Fuzzy Logic MPPT specifically and reported zero steady-state oscillations with faster MPP convergence than either P&O or Incremental Conductance, particularly when irradiance changes quickly.

B. Thermoelectric Energy Recovery

Rowe [5] laid out the theoretical basis for TEG performance: open-circuit voltage is the product of the Seebeck coefficient and the temperature differential across the device, and output power depends on how well that differential is maintained. Kim et al. [6] took this to hardware and measured that rear-surface TEGs on solar panels can contribute 2 to 5 percent of primary PV output under standard test conditions. That sounds small, but it is energy that would otherwise heat the panel and degrade its conversion efficiency, so recovering it improves the system twice over.

C. EV Charging Architectures and Battery Management

Yilmaz and Krein [7] reviewed battery charger topologies for plug-in EVs and noted that single-battery architectures connected to multiple independent sources tend to suffer current instability from simultaneous injection. They did not prescribe a fix, but the implication is clear enough: multi-source systems either need active power management circuitry or architectural separation of the charging paths. This work takes the separation route — simpler to implement and, as the simulation confirms, fully effective at removing the interference. The combination of Fuzzy Logic MPPT, TEG recovery, and a dual battery architecture within one simulation framework has not been widely covered in existing literature [1]–[7], which is the gap this paper addresses.

III. PROPOSED SYSTEM

A. System Overview

The solar PV array is the primary source. Its voltage and current feed the Fuzzy Logic MPPT controller, which computes the power-voltage slope and its rate of change every sample and uses those two values to decide how much to adjust the duty cycle. The adjusted duty cycle drives the PWM generator, which controls the Boost Converter switch. The converter steps up the panel terminal voltage and delivers the boosted output to the main battery. That is the main charging path. In parallel, the TEG — mounted on the panel rear surface — converts the temperature differential between the hot panel face and ambient air into electrical energy. This goes through a blocking diode and into a separate auxiliary battery. The two paths never share a battery terminal. The EV load connects to the main battery; the auxiliary battery provides backup energy when the PV source is unavailable.

B. Block Diagram

© APR 2026 | IRE Journals | Volume 9 Issue 10 | ISSN: 2456-8880
DOI: https://doi.org/10.64388/IREV9I10-1716426

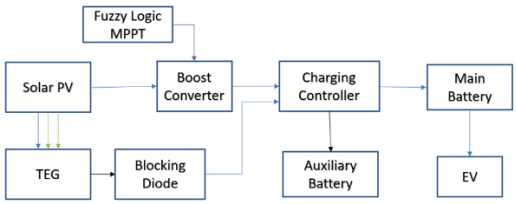

Fig. 1. Block diagram of the proposed solar PV based EV charging station.

Fig. 1 shows the complete topology: Solar PV Array, Fuzzy Logic MPPT Controller, PWM Generator, DC-DC Boost Converter, Thermoelectric Generator, Blocking Diode, Main Battery (PV path), Auxiliary Battery (TEG path), and EV Load.

C. System Working Principle

At each sampling instant the panel voltage V and current I are measured and passed to the Fuzzy MPPT block. A dedicated function inside the block computes E = dP/dV — zero at the MPP, positive to the left, negative to the right — and CE = E(k) − E(k−1), which captures the direction and speed of movement. Both quantities go into the Mamdani fuzzy inference engine, which evaluates the 25-rule base and produces a crisp duty cycle correction ΔD through centroid defuzzification. An integrator accumulates ΔD sample by sample into the running duty cycle D. A saturation block clamps D to [0.05, 0.95] to keep the Boost Converter out of its nonlinear extremes. The clamped D goes to the PWM generator, which produces the gate signal for the converter switch. The converter applies the conversion ratio Vout/Vin = 1/(1−D) and delivers boosted DC to the main battery. The TEG runs continuously in the background; its current flows through the blocking diode to the auxiliary battery, which charges slowly but steadily throughout the simulation.

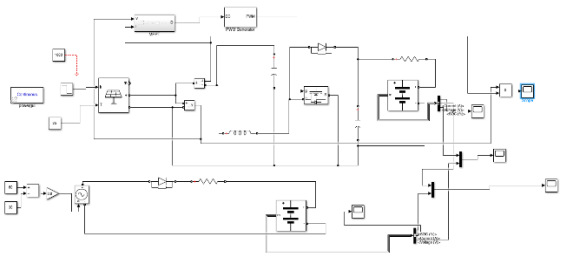

Fig. 2. Complete MATLAB/Simulink model of the proposed system.

Fig. 3. Internal structure of the Fuzzy MPPT subsystem: V and I inputs, E/CE computation, Mamdani FIS block, integrator, and saturation output.

IV. METHODOLOGY

A. Fuzzy Logic MPPT Controller

The first input E = dP/dV tells the controller which side of the MPP the panel is operating on. At the MPP it is zero; moving left of it makes E positive; moving right makes it negative. That tells the controller where it is but not how it got there or how fast things are changing. The second input, CE = E(k) − E(k−1), fills that gap — it is the sample-to-sample change in E, which indicates whether the operating point is converging toward the MPP or drifting away from it. Together, E and CE give the controller enough information to decide both the direction and the magnitude of the correction needed.

E / CE	*E / CE*					
	NB	NS	ZE	PS	PS	PB
NB	NB	NB	NS	ZE	PE	ZE
NS	NB	NB	NS	ZE	PS	PS
ZE	NB	NS	ZE	PS	PS	PB
PS	NS	ZE	PS	PB	PB	PB
PB	ZE	PS	PB	PB	PB	PB

Table I: Fuzzy rule base for MPPT Controller

Both inputs are normalized to [−1, +1] and partitioned into five triangular membership functions: NB (Negative Big), NS (Negative Small), ZE (Zero), PS (Positive Small), and PB (Positive Big). The output ΔD spans [−0.05, +0.05] with the same five labels. The output range was chosen to move the operating point fast enough to track reasonable irradiance changes without overshooting the MPP. The 5×5 rule base gives 25 rules. Three examples illustrate the logic: IF E is ZE AND CE is ZE THEN ΔD is ZE — at the MPP and not drifting, so nothing changes; IF E is PB AND CE is PB THEN ΔD is PB — far left and moving further, so push hard right; IF E is NB AND CE is NB THEN ΔD is NB — far right and moving further, so

© APR 2026 | IRE Journals | Volume 9 Issue 10 | ISSN: 2456-8880
DOI: https://doi.org/10.64388/IREV9I10-1716426

pull hard left. Centroid defuzzification converts the fuzzy output to a crisp number. The result of this structure is that corrections are large far from the MPP, where fast tracking matters, and approach zero at steady state, where ripple elimination matters. A fixed-step controller cannot do both; this one does [4].

B. DC-DC Boost Converter

The Boost Converter steps up the solar panel terminal voltage to a level the battery can use for charging. The conversion ratio is:

$$Vout / Vin = 1 / (1 - D)$$

where Vout is the output voltage, Vin is the panel terminal voltage, and D is the duty cycle from the Fuzzy MPPT controller, kept in the range $0 \leq D < 1$. In this simulation the panel voltage sits near 20 V and the converter steps it up to roughly 715 V at steady state — that is a high duty cycle, deep into the converter's gain region. The MPPT loop keeps updating D in real time so the panel stays at its MPP as conditions change, and the converter turns whatever duty cycle results from that into the corresponding output voltage [8]. Component values for the inductor, capacitor, and switching frequency were set to keep output ripple low while maintaining stable operation across the full duty cycle range.

C. Thermoelectric Generator

The TEG generates voltage from a temperature difference. The governing equation is:

$$V = S \times \Delta T$$

where V is the open-circuit output voltage, S is the Seebeck coefficient of the thermoelectric material in V/K, and ΔT is the temperature difference between the hot and cold faces of the device. In the simulation the TEG is modelled as a controlled voltage source with a hot-side temperature of 60 °C and a cold-side temperature of 30 °C, giving ΔT = 30 °C. Panel surface temperatures of 50 to 65 °C are realistic under 1000 W/m² irradiance depending on wind conditions, so this is a physically reasonable operating point. The blocking diode in series with the TEG output prevents reverse current from the auxiliary battery through the TEG when TEG voltage drops below the battery terminal — at night, during heavy shading, or during startup transients [5], [6].

D. Dual Battery Architecture

The decision to use two separate batteries instead of a shared bank came from watching what happened when only one battery was used. In early simulation runs, the TEG output connected directly to the main battery terminal alongside the Boost Converter output. The oscilloscope showed current spikes at the battery terminal each time the TEG power shifted relative to the PV output — during startup, during the irradiance step, even during small normal fluctuations. These spikes showed up as visible kinks in the SOC curve. In a real battery, that kind of current interference accelerates degradation at the electrode-electrolyte interface and makes the BMS logic unreliable. Giving the TEG its own auxiliary battery, isolated by the blocking diode, removed every one of those spikes. The main battery now sees only clean converter output; the auxiliary battery sees only TEG output. Each SOC curve came out smooth. The auxiliary battery also has a secondary use: it stays charged through whatever residual TEG output the panel temperature differential produces at low irradiance or during early morning hours, so it holds available energy for the EV load even when the main PV source is not producing.

V. SIMULATION SETUP AND RESULTS

A. Simulation Setup

All simulations used standard test conditions from IEC 61215: 1000 W/m² irradiance and 25 °C panel temperature. The TEG ran at 60 °C hot-side and 30 °C cold-side. The Fuzzy MPPT used a 25-rule Mamdani system with ΔD output range [−0.05, +0.05] and duty cycle clamped to [0.05, 0.95]. Total run time was 2 seconds. An irradiance step was applied at t = 1.0 s as a worst-case disturbance test — real cloud transitions are slower than an instantaneous step, so if the system handles this, it will handle the real thing. A variable-step solver was used to capture Boost Converter switching dynamics accurately without forcing an unnecessarily small fixed timestep across the whole run.

B. Boost Converter Output Voltage

Fig. 4 shows two traces: the Boost Converter output voltage in yellow and the panel input voltage in blue. The panel voltage (blue) sits near 20 V throughout and barely moves — the MPPT loop is holding the panel

© APR 2026 | IRE Journals | Volume 9 Issue 10 | ISSN: 2456-8880
DOI: https://doi.org/10.64388/IREV9I10-1716426

at its MPP voltage, so this is expected. The output voltage (yellow) is more interesting. It peaks near 860 V at startup, which is the converter's initial overshoot before the MPPT loop has converged. It then drops and settles through a short oscillatory transient to approximately 715 V by around t = 0.2 s, and holds that level flat with no visible ripple until the irradiance step at t = 1.0 s. The step knocks it down briefly to around 695 V. Recovery is fast — the fuzzy controller detects the shift in E and CE and re-converges quickly, and the voltage stabilizes at the new steady-state level within a fraction of a second. The flat line between t = 0.2 s and t = 1.0 s is worth noting directly: a conventional fixed-step MPPT would keep perturbing the duty cycle even at steady state, producing a small ripple in the output voltage that translates into ripple in the battery charging current. The fuzzy controller produces corrections that approach zero at the MPP, so the voltage trace is genuinely flat rather than just low-ripple.

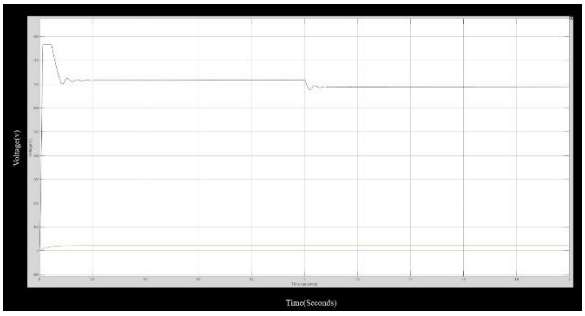

Fig. 4. Boost Converter output voltage (~715 V steady-state, yellow) and panel input voltage (~20 V, blue). Startup peak near 860 V settles by t = 0.2 s; brief dip to ~695 V at t = 1.0 s recovers within a fraction of a second.

C. Solar PV Output Power

Fig. 5 shows PV output power in units of $\times 10^5$ W. The startup transient produces a single peak as the Fuzzy MPPT moves the operating point from its initial position to the MPP. One peak, then flat — that is the distinguishing characteristic of fuzzy control compared to fixed-step P&O, which would produce several oscillating peaks before settling. After the initial transient, power holds at a steady flat value with no ripple until the irradiance step at t = 1.0 s causes a brief dip. Recovery is quick, and the output settles at the new MPP level with minimal undershoot. The single-peak startup response directly results from the large ΔD corrections the rule base applies when E and CE are both large: the operating point gets pushed to the vicinity of the MPP in fewer steps than a fixed-step algorithm would take.

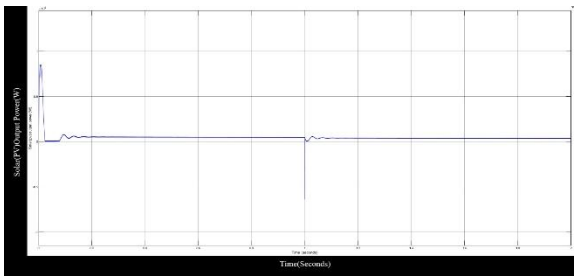

Fig. 5. PV output power under Fuzzy Logic MPPT: single-peak startup transient followed by flat steady-state with zero ripple. Brief disturbance at t = 1.0 s recovers quickly.

D. Main Battery State of Charge

Fig. 6 shows the main battery SOC rising from about 51.5% at the start to about 55% by the end of the 2-second run. The curve is a straight line — no kinks, no oscillations, no flattening. This is what a clean charging current looks like when it integrates into a SOC trace. The smoothness is a direct consequence of the ripple-free power delivery from the Fuzzy MPPT system. With a fixed-step controller, steady-state power ripple would flow through the Boost Converter and appear as a small but measurable ripple in battery charging current, which would show up as a slightly irregular SOC curve. There is none of that here. The irradiance step at t = 1.0 s leaves no visible mark on the SOC curve either — the recovery in power output is fast enough that the accumulated effect on battery charge is negligible.

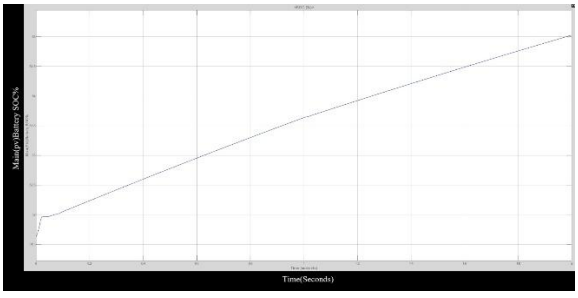

Fig. 6. Main battery SOC: smooth linear rise from ~51.5% to ~55% over 2 seconds, with no oscillation or disturbance response visible.

E. Auxiliary Battery State of Charge

Fig. 7 shows the auxiliary battery SOC rising from approximately 41.97% to approximately 42.015%

© APR 2026 | IRE Journals | Volume 9 Issue 10 | ISSN: 2456-8880
DOI: https://doi.org/10.64388/IREV9I10-1716426

over the same 2-second window — an increase of roughly 0.045 percentage points against the main battery's 3.5 percentage points. The slow rate reflects the TEG's output relative to the PV array. At $\Delta T = 30$ °C the TEG contributes a few percent of PV output power, consistent with Kim et al. [6]. What the curve lacks in steepness it makes up for in quality: it is smooth from start to finish, with no spikes, no irregularities, and no sign of anything crossing over from the main charging path. This is the isolation result. In the earlier single-battery runs, kinks from the main path transients were visible in the shared SOC trace. Here they are completely absent, because the two paths are not sharing a terminal. The slow but steady auxiliary charging also means the auxiliary battery retains a useful state of charge during periods of reduced solar availability — which is its purpose in the design.

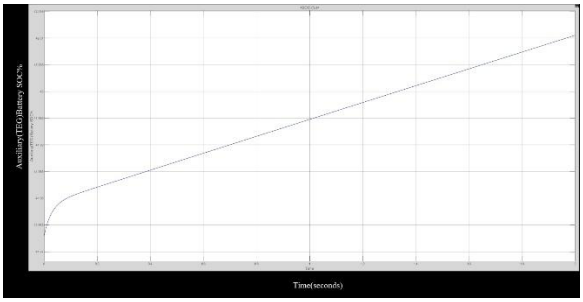

Fig. 7. Auxiliary battery SOC: slow but smooth and continuous rise from ~41.97% to ~42.015%, charged exclusively by the TEG with no cross-path interference.

F. Combined Battery Current

Fig. 8 puts both battery currents on the same time axis — main battery in yellow, auxiliary in blue. Both settle to stable negative values, meaning both are in continuous charging mode throughout the run. The sign convention here is the Simulink battery block standard where charging current is negative. The main battery current (yellow) shows the startup transient in the first 0.2 seconds, then settles flat. At t = 1.0 s, both traces show a brief perturbation from the irradiance step and both return to steady state quickly. The important thing to look for in this plot is coupling between the traces — a spike in one appearing as a disturbance in the other. It is not there. During the yellow trace startup transient, the blue trace is already settled. During the t = 1.0 s perturbation, each trace responds to its own source and then recovers independently. This is the dual battery result in its most direct form: two charging paths, two batteries, no shared terminal, no interference.

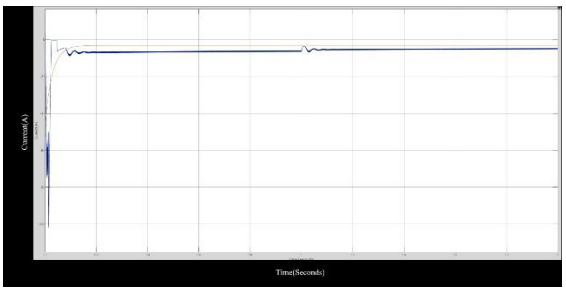

Fig. 8. Combined battery current: both traces settle to stable negative (charging) values independently, with no cross-source coupling visible across the full simulation.

G. Performance Summary

Parameter	Conventional Fixed-Step	Proposed Fuzzy Logic	Result in Simulation
Startup transient	Multiple oscillating peaks	Single peak only	Faster convergence to MPP
Steady-state power ripple	Persistent, unavoidable	Zero	More energy extracted
Converter output voltage	Small ripple at steady state	Flat at ~715 V	Cleaner battery charging
Disturbance recovery	Slow re-convergence	Near-instant	Handles real-world irradiance variation
TEG path stability	Spikes on shared battery	Isolated: no spikes	Cross-source interference eliminated
Main battery SOC	Irregular curve	Straight line	Predictable charging behavior

Auxiliary battery SOC	N/A	Slow, smooth rise	Backup charge maintained

Table II. Proposed Fuzzy Logic system versus conventional fixed-step methods across all five simulation outputs.

VI. DISCUSSION

The five output waveforms together tell a more complete story than any one of them does alone. Start with the converter voltage and the PV power output — they are the same result viewed from different angles. The flat steady-state in both is the fuzzy controller applying near-zero corrections once E and CE both approach zero at the MPP. A fixed-step controller keeps perturbing at steady state regardless of where it is on the curve, so its power output and converter voltage both carry a persistent ripple. That ripple is small, but it propagates through the system: ripple in converter voltage becomes ripple in charging current, which over hundreds of charge cycles stresses the battery electrode-electrolyte interface and reduces cell life. The fuzzy result removes that source of degradation entirely.

The voltage graph is worth a specific comment because papers on MPPT often focus on power tracking efficiency and leave voltage behavior unreported. Here the converter output starts near 860 V, settles to 715 V by around t = 0.2 s, dips to roughly 695 V at the irradiance step, and recovers. The settling time is fast. The post-settling trace is flat. These are not incidental results — they follow directly from the rule base structure. When E and CE are both large, the controller pushes hard. When both are near zero, it barely moves. The voltage waveform reflects that logic precisely.

The dual battery result is straightforward to read in Fig. 8. The two current traces move independently throughout the run. During the yellow startup transient, the blue trace shows nothing. During the t = 1.0 s perturbation, each trace responds to its own source and recovers on its own schedule. This is because the two paths have no shared terminal — the blocking diode ensures that any change in TEG output does not appear at the main battery terminal, and vice versa. The earlier single-battery simulation showed the problem directly: spikes in the SOC curve each time the two source power levels shifted relative to each other. Separating the paths removed every one of them.

One limitation is worth stating clearly. The simulation uses constant irradiance for the first second and then an instantaneous step — not a realistic irradiance profile. Real solar irradiance varies continuously, with cloud transitions that typically unfold over several seconds rather than instantaneously. The step test is a worst-case scenario, and if the fuzzy controller handles it with near-instant recovery, it will handle slower real-world transitions more easily. But tracking efficiency under a recorded real-irradiance input would be a more rigorous validation, and that is planned as part of hardware prototyping where actual panel measurements can drive the algorithm.

The TEG contribution is small in absolute terms — 0.045 percentage points of auxiliary SOC against 3.5 percentage points of main SOC over 2 seconds. Some readers may question whether the added complexity is worth it. The answer depends on what the auxiliary battery is for. It is not meant to carry the main charging load. It is there to stay charged during periods when the PV source is unavailable — heavy clouds, early morning, evening — and provide backup energy to the EV load. Continuous trickle charging from the TEG, even at 2 to 5 percent of PV output, keeps the auxiliary battery above a useful state of charge between high-irradiance periods. That is a practical benefit for an off-grid or partially off-grid charging station, even if the numbers look modest on a 2-second simulation trace.

VII. CONCLUSION

This paper built and simulated a solar PV based EV charging station that addresses two specific problems in conventional designs. Fixed-step MPPT oscillates at steady state and wastes energy indefinitely; replacing it with a 25-rule Fuzzy Logic controller produced a single startup transient, zero steady-state power ripple, and a flat Boost Converter output voltage that settled to roughly 715 V and recovered quickly from a worst-case irradiance step. Connecting a TEG to a shared main battery introduces current

© APR 2026 | IRE Journals | Volume 9 Issue 10 | ISSN: 2456-8880
DOI: https://doi.org/10.64388/IREV9I10-1716426

spikes from simultaneous multi-source charging; routing TEG output to a dedicated auxiliary battery through a blocking diode removed the interference and produced smooth, independent SOC progression in both batteries. All five simulation outputs — PV power, converter voltage, main SOC, auxiliary SOC, and combined battery current — confirmed that the proposed system performs better than a conventional single-source fixed-step architecture on every metric that was tested. The system is ready for hardware prototyping, and the simulation results give a clear baseline to validate against.

VIII. FUTURE SCOPE

The fuzzy membership function parameters in this work were tuned manually. Replacing that with a Grey Wolf Optimizer or Particle Swarm Optimization would automate the tuning process and could find parameter sets better suited to specific panel characteristics or local irradiance patterns, without changing the fuzzy control structure itself. This is a natural first step for anyone building on this simulation.

The auxiliary battery in the current design is passive — it takes whatever the TEG delivers. Adding a bidirectional DC-DC converter between the two batteries would allow active energy transfer: the auxiliary battery could supplement the main battery during high-demand charging events, and the main battery could top up the auxiliary during idle periods. This turns the dual battery arrangement from an isolation mechanism into an active buffer, which is more useful in a real deployment.

Smart grid integration would allow the EV battery to return stored energy to the grid during peak demand and receive compensation in return. The PV and storage infrastructure in this design provides a reasonable base for that extension. On the validation side, running the simulation against a recorded real-irradiance time series — rather than the constant-then-step profile used here — would give a more honest picture of tracking efficiency under real conditions. Hardware prototyping on a bench-scale setup with actual panels, TEG modules, and a microcontroller-based fuzzy implementation would then provide the experimental data needed to verify whether the simulation predictions hold up in practice.

Rule No.	IF Condition (E, CE)	THEN Output (ΔD)
R1	E is NB AND CE is NB	ΔD is NB (Large negative correction)
R2	E is NB AND CE is NS	ΔD is NB (Large negative correction)
R3	E is NB AND CE is ZE	ΔD is NM (Medium negative correction)
R4	E is NB AND CE is PS	ΔD is NS (Small negative correction)
R5	E is NB AND CE is PB	ΔD is ZE (No correction)
R6	E is NS AND CE is NB	ΔD is NB (Large negative correction)
R7	E is NS AND CE is NS	ΔD is NM (Medium negative correction)
R8	E is NS AND CE is ZE	ΔD is NS (Small negative correction)
R9	E is NS AND CE is PS	ΔD is ZE (No correction)
R10	E is NS AND CE is PB	ΔD is PS (Small positive correction)
R11	E is ZE AND CE is NB	ΔD is NS (Small negative correction)
R12	E is ZE AND CE is NS	ΔD is NS (Small negative correction)
R13	E is ZE AND CE is ZE	ΔD is ZE (At MPP — no correction)
R14	E is ZE AND CE is PS	ΔD is PS (Small positive correction)
R15	E is ZE AND CE is PB	ΔD is PS (Small positive correction)
R16	E is PS AND CE is NB	ΔD is NS (Small negative correction)
R17	E is PS AND CE is NS	ΔD is ZE (No correction)
R18	E is PS AND CE is ZE	ΔD is PS (Small positive correction)
R19	E is PS AND CE is PS	ΔD is PM (Medium positive correction)
R20	E is PS AND CE is PB	ΔD is PB (Large positive correction)
R21	E is PB AND CE is NB	ΔD is ZE (No correction)
R22	E is PB AND CE is NS	ΔD is PS (Small positive correction)
R23	E is PB AND CE is ZE	ΔD is PM (Medium positive correction)
R24	E is PB AND CE is PS	ΔD is PB (Large positive correction)
R25	E is PB AND CE is PB	ΔD is PB (Large positive correction)

Table III: COMPLETE 25-RULE BASE OF THE MAMDANI FUZZY LOGIC MPPT CONTROLLER

REFERENCES

[1] T. Esram and P. L. Chapman, "Comparison of Photovoltaic Array Maximum Power Point Tracking Techniques," IEEE Trans. Energy Convers., vol. 22, no. 2, pp. 439–449, Jun. 2007.

[2] N. Femia, G. Petrone, G. Spagnuolo, and M. Vitelli, "Optimization of Perturb and Observe Maximum Power Point Tracking Method," IEEE Trans. Power Electron., vol. 20, no. 4, pp. 963–973, Jul. 2005.

[3] B. Subudhi and R. Pradhan, "A Comparative Study on Maximum Power Point Tracking Techniques for Photovoltaic Power Systems," IEEE Trans. Sustain. Energy, vol. 4, no. 1, pp. 89–98, Jan. 2013.

[4] H. Rezk and A. M. Eltamaly, "A Comprehensive Comparison of Different MPPT Techniques for Photovoltaic Systems," Sol. Energy, vol. 112, pp. 1–11, Feb. 2015.

[5] D. M. Rowe, Thermoelectrics Handbook: Macro to Nano. Boca Raton, FL: CRC Press, 2006.

[6] S. Kim, M. Kim, and J. Park, "Waste Heat Harvesting from Solar Panels Using

Thermoelectric Generators," Energy Convers. Manag., vol. 75, pp. 461–467, 2013.

[7] M. Yilmaz and P. T. Krein, "Review of Battery Charger Topologies, Charging Power Levels, and Infrastructure for Plug-In Electric and Hybrid Vehicles," IEEE Trans. Power Electron., vol. 28, no. 5, pp. 2151–2169, May 2013.

[8] N. Mohan, T. M. Undeland, and W. P. Robbins, Power Electronics: Converters, Applications and Design, 3rd ed. New York, NY: Wiley, 2003.

[9] M. H. Rashid, Power Electronics Handbook: Devices, Circuits, and Applications, 3rd ed. Oxford: Elsevier, 2014.

[10] IEEE Standard 1547-2018, Standard for Interconnection and Interoperability of Distributed Energy Resources. New York, NY: IEEE, 2018.

[11] MathWorks, "Simscape Electrical: Battery Block Reference," MathWorks Documentation. [Online]. Available: https://www.mathworks.com/help/simscape/electrical